Spin dynamics of EuO in the paramagnetic phase

R. Chaudhury and B. S. Shastry

Tata Institute of Fundamental Research, Colaba, Bombay 400005, India

(Received 26 June 1987; revised manuscript received 7 December 1987)

The spin dynamics of the semiclassical Heisenberg model on the fcc lattice, with ferromagnetic interactions up to the second-nearest-neighbor shell, is studied in the paramagnetic phase at the temperatures $1.68T_c$ and $2.0T_c$ using the Monte Carlo–molecular-dynamics technique. The important quantities calculated are the dynamic structure function $S(q,\omega)$, the spin autocorrelation function $\langle S_i(0) \cdot S_i(t) \rangle$, and the static correlation functions. Our results for $S(q,\omega)$ show the existence of purely diffusive modes in the low-q regime. For q close to the zone boundary, our calculated $S(q,\omega)$ shows a three-peak structure, signifying damped propagating modes. This result disagrees with the earlier experimental observation of Mook and the theoretical result of Lindgard, where a two-peak structure was obtained near the zone boundary. Our results for $S(q,\omega)$ in the entire q space are in good qualitative and quantitative agreement with the recent neutron scattering experiments by Böni and Shirane and also with the predictions of Young and Shastry. Our calculated autocorrelation function shows a diffusive behavior temporally.

I. INTRODUCTION

Recent neutron scattering experiments on europium chalcogenides (EuO and EuS), by Böni and Shirane,[1] have provided valuable detailed information on the spin dynamics in these materials, which are well-characterized realizations of the three-dimensional (3D) isotropic Heisenberg model. This model, despite its simplicity of statement, is of great complexity and the various approximate analytical treatments that appear in literature[2,3] are very often difficult to assess and evaluate. The only reliable way, at present, to calculate the spin dynamics of the Heisenberg model is the technique of the Monte Carlo simulation coupled with the molecular dynamics (MCMD). We have been motivated by the recent experiments to study the spin dynamics of the paramagnetic EuO and EuS by the MCMD technique. We present, in this paper, the resulting spin correlations for EuO, which agree remarkably well with the recent experimental results in most features. We also present the spin autocorrelation functions $\langle S_i(0) \cdot S_i(t) \rangle$ which are accessible to the local probes, such as perturbed angular correlation (PAC), muon spin rotation (μ^+SR), and electron spin resonance (ESR), in the hope of stimulating further experiments. Besides these, we also calculate the static spin correlations in real space as well as in q space.

The main point which emerges from this study is that the structure function $S(q,\omega)$ has interesting and nontrivial structure in the paramagnetic phase and departs greatly from the Lorentzian or semi-Lorentzian (spin diffusion) shape forced at small q by the global spin conservation laws. Noticeable shoulders at finite values of ω appear for large enough q and may be interpreted as (damped) propagating modes—these are indeed the results of the nonlinearity of the equations of the spin dynamics rather than of any significant equilibrium (static) correlations. The frequencies of the propagating modes obtained in our calculation are quite similar to those

found in the approximate analytical calculations of Young and Shastry (YS) (Ref. 4) and also of Lindgard.[5] The calculation of YS makes use of the three-pole ansatz following the earlier work of Shastry, Edwards, and Young (SEY),[6] whereas the calculation of Lindgard is similar to a two-pole theory. These theoretical characteristic frequencies are also fairly close to those obtained in the earlier experimental work on the paramagnetic EuO in the single-crystal form by Mook.[7] However, one important difference between these results was that while in Lindgard's calculation and in Mook's experimental result, $S(q,\omega)$ in the propagating regime of q showed only a two-peak structure with no appearance of a central peak; YS found a three-peak structure for $S(q,\omega)$ with a pronounced central peak. In order to resolve the apparent anomaly in the shape of $S(q,\omega)$ in the propagating regime and to test the existing analytic theories in a more quantitative way, Böni and Shirane carried out detailed measurements on the paramagnetic EuO using neutrons. They determined the temperature-independent background contributions from the nonmagnetic scattering very accurately by performing experiments in the ordered phase, and this enabled them to filter out the pure magnetic part of the scattering cross section quite reliably even in the paramagnetic phase. They have also followed the procedure of Wicksted et al.[1] to determine the magnetic form factor very accurately and extract the energy integrated pure magnetic structure function $S(q)$ on an absolute scale. Their experiments were performed on the powder form of EuO and their measurements yield pseudostatic correlation functions [energy integrated $S(q,\omega)$ over a sufficiently large energy window] on an absolute scale, producing a rms value of the local moment in good agreement with the expected one ($S \sim \frac{7}{2}$). The results of Böni and Shirane showed the existence of a three-peak structure for $S(q,\omega)$ with the appearance of a central peak in the propagating regime in q space, in agreement with the predictions of the YS theory. It

seems now that the inaccurate subtraction of the non-magnetic background scattering might have distorted the shape of the magnetic structure function in Mook's observation.

The results of Böni and Shirane inspired us to calculate $S(q,\omega)$ in the paramagnetic phase of the Heisenberg model, with parameters appropriate to EuO, using the MCMD technique. Our results confirm the existence of a three-peak structure for $S(q,\omega)$ in the propagating regime. In fact, our plan includes the study of spin dynamics in the paramagnetic phases of EuS and EuSe as well. In all of these rare-earth chalcogenide systems which are insulators, the magnetic ion Eu^{+2} forms a fcc lattice and the exchange interaction is confined to the first- and second-neighbor shells only. In all these systems the Eu^{+2} ion is in spin $\frac{7}{2}$ state and the orbital effects are quenched completely since the magnetism is due only to the electrons of exactly half-filled f shell. In EuO both the first-neighbor interaction and the second-neighbor interaction are ferromagnetic; in EuS and EuSe the first-neighbor interaction is ferromagnetic but the second-neighbor interaction is antiferromagnetic. EuO and EuS order ferromagnetically and EuSe orders antiferromagnetically. We only report the work done for EuO in this paper. The work done for EuS will be reported in another publication[8] soon. We present the $S(q,\omega)$ results on an absolute scale for EuO at two temperatures, viz. $1.68T_c$ and $2.0T_c$ and compare these with the available experimental data as well as with the results of some approximate theories. Ours are, we believe, the first such computations for more than nearest-neighbor models. The technique used here is an adaptation of the recent simulation of Shastry[9] to the case of the fcc lattice with further-neighbor interactions.

The plan of the paper is as follows: In Sec. II we briefly mention the existing theoretical approaches and summarize some of the recent relevant experiments; in Sec. III we describe the MCMD technique and the procedure of our calculation in some details; in Sec. IV we display all the important results of our simulation and also compare our results with the results of other theoretical approaches and experiments; and finally, in Sec. V we discuss some implications of our results.

II. BRIEF REVIEW OF APPROXIMATE THEORIES AND EXPERIMENTS RELATING TO EuO

Several analytic approximate techniques have been tried to probe the spin dynamics in the paramagnetic phase of the 3D isotropic Heisenberg model. Some of the well-known analytic approaches are SEY three-pole theory,[6] Lindgard's correlation theory,[5] diagrammatic perturbation theory by Resibois and De Leener,[10] asymptotic renormalization-group technique by Folk and Iro,[11] and high-temperature series expansion technique.[12] The mode coupling theories developed by Kawasaki[13] and Blume and Hubbard[14] are similar to the work of Resibois and De Leener. These theories are rather successful in the predictions for dynamical critical indices. However, the shape functions obtained in the treatments of Kawasaki and of Blume and Hubbard are monotonic

even in the large-q regime (except at the zone boundary), whereas in the work of Resibois and De Leener the shape functions do not show purely diffusive behavior even for very low values of q at temperatures close to the critical point. These features do not conform to the ones found in most paramagnets. Reiter[15] later used an approach similar to that of Resibois and De Leener, but treated the coupling between the modes more accurately. His treatment has been quite successful in explaining the experimentally observed spin dynamics of $RbMnF_3$, a 3D Heisenberg antiferromagnet, in the paramagnetic phase. The work of Folk and Iro[11] predicts the deviation of the shape function from a pure Lorentzian form for slightly higher values of q within the diffusive regime. This is supported by the experimental results of Böni and Shirane for paramagnetic EuO. For convenience we discuss briefly the YS (or SEY) theory and Lindgard's theory and give the corresponding results for EuO.

The SEY theory makes use of the three-pole approximation of Lovesey and Meserve[16] in the moment expansion, or the continued fraction expansion scheme of Mori,[17] and also uses the spherical model[18] approximation to calculate the various static quantities occurring in the expansion. The results of the calculation of YS performed for the paramagnetic EuO show the existence of damped propagating modes close to the zone boundary and the existence of diffusive modes for low q. More precisely, the dynamic structure function $S(q,\omega)$, when plotted in the constant q scans as a function of ω, shows a three-peak structure consisting of a central peak and two peaks at positive and negative values of ω for q close to the zone boundary; however, for low q it shows only a central peak. Qualitatively, the ratio r of the fourth moment to the second moment squared determines the shape; it is diffusive (one peak) if $r \geq 3$ and has a propagating character if $r < 3$.

The shape function given by YS has the form

$$F(q,\omega) = \frac{1}{\pi} \frac{\tau\delta_1\delta_2}{\omega^2\tau^2(\omega^2-\delta_1-\delta_2)^2+(\omega^2-\delta_1)^2} \; ,$$

where,

$$\delta_1 = \langle \omega^2 \rangle_q \; ,$$

$$\delta_1\delta_2 = \langle (\omega^2 - \langle \omega^2 \rangle_q)^2 \rangle_q \; ,$$

and

$$\tau = (\pi\delta_2/2)^{-1/2} \; .$$

Lindgard's theory is a self-consistent correlation theory of one dynamical variable. It is, in fact, equivalent to a two-pole approximation to the continued fraction expansion scheme of Mori. The results for the paramagnetic EuO, produced by this theory, show a two-peak structure in $S(q,\omega)$ with no central peaks, for q close to the zone boundary; whereas for low q, the results only show a central peak for $S(q,\omega)$.

The shape function given by Lindgard's theory has the form

$$F(q,\omega) = \frac{1}{\pi} \frac{\delta_1\beta}{(\omega^2-\delta_1)^2+\omega^2\beta^2} \quad \text{for} \quad \omega \leq \omega_c \; ,$$

where $\delta_1 = \langle \omega^2 \rangle$ and β is the damping parameter which is determined from self-consistent equations. The cutoff frequency ω_c is determined from the moment relations.

There have been inelastic neutron scattering experiments on the paramagnetic EuO by several experimental groups. Mook was one of the pioneers to perform neutron scattering experiments on a single crystal of EuO in the paramagnetic phase. His experiments probed the $\langle 111 \rangle$ direction only. His observed $S(q,\omega)$ in the constant q scans, showed distinct broad peaks at finite values of ω with no occurrence of central peaks for q close to the zone boundary. In the rest of the q space the curves only showed a central peak.

Recently, Böni and Shirane have performed more careful and accurate neutron scattering experiments on the EuO powder. Because of the high isotropy in its magnetic properties, the powder form of EuO is expected to show very similar results as the single-crystal form.[1] Böni and Shirane's measurements also confirmed the existence of damped propagating modes close to the zone boundary and the existence of diffusive modes in the rest of the q space. But their observed $S(q,\omega)$, for q close to the zone boundary, shows a three-peak structure contrary to the two-peak structure observed in Mook's observations. Until now PAC or ESR or μ^+SR experiments have not been performed on EuO, so there are no experimental results for the spin autocorrelation function of EuO.

III. THE MCMD APPROACH AND CALCULATIONS

The 3D isotropic quantum Heisenberg model with nearest- and next-nearest neighbor interactions, as is relevant for our problem, is defined as

$$\hat{\mathcal{H}} = -\sum_{\substack{\langle i,j \rangle \\ \langle\langle i,j \rangle\rangle}} J_{ij} \hat{\mathbf{S}}_i \cdot \hat{\mathbf{S}}_j \ , \tag{3.1}$$

where the symbol $\langle i,j \rangle$ indicates that the ith and the jth sites are nearest neighbors, and the symbol $\langle\langle i,j \rangle\rangle$ indicates that the ith and the jth sites are next-nearest neighbors; the sum goes over the entire 3D lattice.

Also, $J_{ij} = J_1$, when i and j are nearest neighbors and $J_{ij} = J_2$, when i and j are next-nearest neighbors. For EuO, $J_1 > J_2 > 0$.

The dynamics of the spins are governed by the equations

$$\frac{d\hat{\mathbf{S}}_i}{dt} = \frac{1}{i\hbar} [\hat{\mathbf{S}}_i, \hat{\mathcal{H}}] \ ,$$

where the square bracket denotes the commutator. The equations of motion are

$$\frac{d\hat{\mathbf{S}}_i}{dt} = \frac{1}{\hbar} \sum_j J_{ij} (\hat{\mathbf{S}}_i \times \hat{\mathbf{S}}_j) \ . \tag{3.2}$$

The quantities of special interest are the static correlation functions in real space as well as in q space, the autocorrelation function, and the dynamic structure function. All these thermodynamic quantities involve canonical ensemble averages. Since the equations of spin dynamics, mentioned above, have two conserved quantities, viz. the

energy and the magnetization, one has to use a combination of the Monte Carlo (MC) and the molecular dynamics (MD) techniques to find the estimates for the quantities of interest.

Now let us give the definitions of some of the relevant quantities in our calculation. The lattice Fourier transforms of the real space spin configuration are defined by

$$\hat{\mathbf{S}}_q(t) = \frac{1}{\sqrt{N}} \sum_i \hat{\mathbf{S}}_i(t) e^{-i\mathbf{q}\cdot\mathbf{r}_i} \ , \tag{3.3}$$

where N is the total number of spins, i.e., the total number of sites in the finite system. In our case of a fcc lattice $N = 4L^3$, where L is the length (in units of the lattice parameter a) of the finite system taken in the form of a cubical box. This $\hat{\mathbf{S}}_q(t)$ is a fundamental quantity in the problems involving spin dynamics, which is calculated by the MD technique. The static q space spin-spin correlation function is defined as

$$C_q(0) = \langle \hat{\mathbf{S}}_q(0) \cdot \hat{\mathbf{S}}_{-q}(0) \rangle \ , \tag{3.4}$$

where $\langle\ \rangle$ denotes here the ensemble average. Another quantity of importance is the static real space spin-spin correlation function, given by

$$C(\mathbf{r},0) = \frac{1}{N} \sum_q C_q(0) e^{i\mathbf{q}\cdot\mathbf{r}}$$

$$= \langle \hat{\mathbf{S}}_i(0) \cdot \hat{\mathbf{S}}_{i+r}(0) \rangle \ . \tag{3.5}$$

Now let us introduce the dynamic quantities of interest, which we calculate. The spin autocorrelation function is given by

$$C(0,t) = \langle \hat{\mathbf{S}}_i(0) \cdot \hat{\mathbf{S}}_i(t) \rangle \ . \tag{3.6}$$

The most important quantity from the theoretical as well as from the experimental point of view, is the dynamic structure function. It is defined as

$$S(q,\omega) = \frac{1}{2\pi} \int_{-\infty}^{+\infty} C_q(t) e^{i\omega t} dt \ ,$$

where

$$C_q(t) = \langle \hat{\mathbf{S}}_q(0) \cdot \hat{\mathbf{S}}_{-q}(t) \rangle \ . \tag{3.7}$$

Another quantity which occurs directly in various analytic approximate theories is the relaxation shape function. It is given by

$$F(q,\omega) = \frac{1}{2\pi} \int_{-\infty}^{+\infty} [C_q(t)/C_q(0)] e^{i\omega t} dt \ . \tag{3.8}$$

Thus we have an immediate relation

$$S(q,\omega) = F(q,\omega) C_q(0) \ . \tag{3.9}$$

Now we make a semiclassical approximation, viz. we replace the operator $\hat{\mathbf{S}}_i$ by a classical vector of length $\sqrt{S(S+1)}$, where S is the magnitude of the spin on each site. This semiclassical approximation is fairly good for high-temperature and high-spin value. So the semiclassical Heisenberg Hamiltonian becomes

$$\mathcal{H} = -S(S+1) \sum_{\substack{\langle i,j \rangle \\ \langle\langle i,j \rangle\rangle}} J_{ij} \mathbf{s}_i \cdot \mathbf{s}_j \ , \tag{3.10}$$

where s_i is a classical unit vector at the ith site. Similarly, all the other previous expressions undergo corresponding changes under the semiclassical approximation (correspondence)

$$\hat{\mathbf{S}}_i \rightarrow \mathbf{s}_i \sqrt{S(S+1)} \ .$$

This semiclassical approximation has been made to enable us to make use of the classical Monte Carlo–molecular-dynamics technique for our calculation. Using this technique we get an estimate of the classical dynamic structure function $S_{cl}(\mathbf{q},\omega)$. To recover the true quantum mechanical $S(\mathbf{q},\omega)$, denoted by $S_{QM}(\mathbf{q},\omega)$, we make use of a prescription by Windsor[19]

$$S_{QM}(\mathbf{q},\omega) = \frac{2S_{cl}(\mathbf{q},\omega)}{1+\exp(-\hbar\omega/kT)} \ . \quad (3.11)$$

This $S_{QM}(\mathbf{q},\omega)$ satisfies the detailed balance condition, as is required in the thermal equilibrium. Moreover, the frequency integral of $S_{QM}(\mathbf{q},\omega)$ is exactly equal to the frequency integral of $S_{cl}(\mathbf{q},\omega)$, which gives the static q-space correlation function $C_q(0)$ (in Appendix A we provide a brief discussion of the rationale behind this prescription). The computed classical structure function then gives an estimate of the quantum function.

We use the Metropolis method[20,21] for the MC. This MC updating can in general be done in the following three different ways: (1) Sequential updating, (2) random updating, (3) sequential random updating. We have used the sequential updating procedure in our calculation. Since we are dealing with a finite system, we will have to impose a suitable spatial boundary condition. We have taken the periodic boundary condition for our calculation.

We perform the MC calculation in the following way: we start from an infinite-temperature configuration and perform 3000 MC steps/spin. We store the final spin configuration thus obtained at a given temperature. Then we go on performing further MC operations and store the spin arrays after every 1000 MC steps/spin. We store altogether 10 arrays of MC ages between 3000 MC steps/spin and 12 000 MC steps/spin. These arrays are to be used as the initial conditions for the MD. Now to ensure the attainment of thermal equilibrium after 3000 MC steps/spin, we study certain static properties. We look for the steady values of the averages and of the rms fluctuations in the estimates of $C_q(0)$'s obtained from a reasonably large set of configurations generated by the MC operations. We found that by making estimates from sets of 1000 configurations (two successive configurations in a set differing by 2 MC steps/spin) each, we achieve practically a steady average and a steady rms fluctuation in $C_q(0)$'s for all the allowed q values examined along the $\langle 111 \rangle$ direction. Also the ratios of the steady rms fluctuations to the steady averages for various q values are very close to the values expected in the thermal equilibrium (see Appendix B). Moreover, these steady averages for various q values can be parametrized very well with the Ritchie-Fisher functional form[22,9] of the high-temperature series expansion results for the 3D Heisenberg model [with $C_q(0)$ being written simply as C_q],

$$C_q = \frac{\alpha(\beta+\gamma\psi_q)^{\eta/2}}{(\beta+\psi_q)} \ , \quad (3.12)$$

where

$$\eta = \tfrac{2}{45} \ , \quad (3.13)$$

and for a 3D fcc lattice with nearest-neighbor and next-nearest-neighbor interactions,

$$\psi_q = \psi_{1q} + \psi_{2q}\phi \ , \quad (3.14)$$

where

$$\phi = \frac{J_2}{2J_1} \ , \quad (3.15)$$

$$\psi_{1q} = 1 - \frac{1}{3}\left[\cos\frac{q_x a}{2}\cos\frac{q_y a}{2} + \cos\frac{q_y a}{2}\cos\frac{q_z a}{2} \right. $$
$$\left. + \cos\frac{q_z a}{2}\cos\frac{q_x a}{2} \right] \ , \quad (3.16)$$

$$\psi_{2q} = 1 - \tfrac{1}{3}[\cos(q_x a)+\cos(q_y a)+\cos(q_z a)] \ , \quad (3.17)$$

where a is the lattice parameter,

$$\gamma = \frac{(5-\eta)}{3} \ ,$$

$$C_{q=0} = \alpha\beta^{\eta/2-1} \ ,$$

ξ is the correlation length,

$$\xi = a[(1+2\phi)/12\beta]^{1/2}$$

(see Appendix C). We also find the stabilization of both the average energy and the rms fluctuation in the energy, when the averaging is done over sets of 1000 configurations each, starting from the MC age of 3000 MC steps/spin, as described earlier. Besides, the ratio of the rms fluctuation to the average value is of the order of $1/\sqrt{N}$, as expected in the thermal equilibrium. We also calculate directly the steady average value of the real space spin-spin correlations $C(r)$'s, taking into account the averaging over all the lattice points and also the averaging over all the possible directions, relevant for a particular neighbor shell, up to the fourth-neighbor shell; these agree very well with the corresponding values obtained by Fourier transforming C_q's and then averaging over all the possible directions, as is relevant for that particular neighbor shell. This shows the existence of the thermal equilibrium as well as the correctness of the algorithms used in our calculation.

Now turning to the MD calculations, we performed the dynamical runs with each of the 10 stored arrays as the initial conditions. Under the semiclassical approximation, as mentioned earlier, the Heisenberg's equation of motion becomes[23]

$$\frac{d\mathbf{s}_i}{dt} = \hbar^{-1}\sqrt{S(S+1)}\sum_j J_{ij}(\mathbf{s}_i \times \mathbf{s}_j) \quad \text{for} \quad i=1,N \ . \quad (3.18)$$

For our model appropriate to EuO,

$$\frac{d\mathbf{s}_i}{dt} = \hbar^{-1}J_1\sqrt{S(S+1)}\left[\sum_{j\in\text{first-neighbor shell}}(\mathbf{s}_i\times\mathbf{s}_j)+\left[\frac{J_2}{J_1}\right]\sum_{j\in\text{second-neighbor shell}}(\mathbf{s}_i\times\mathbf{s}_j)\right].\tag{3.19}$$

From this equation we can define a natural time unit in our problem t_0, where

$$t_0^{-1}=\hbar^{-1}J_1\sqrt{S(S+1)}.$$

Therefore

$$\frac{d\mathbf{s}_i}{dt} = t_0^{-1}\left[\sum_{j\in\text{first-neighbor shell}}(\mathbf{s}_i\times\mathbf{s}_j)+\left[\frac{J_2}{J_1}\right]\sum_{j\in\text{second-neighbor shell}}(\mathbf{s}_i\times\mathbf{s}_j)\right],\quad\text{for}\quad i=1,N.\tag{3.20}$$

Considering the equations of motion for each of the x,y,z components separately, we have $3N$ coupled nonlinear differential equations to be solved. We integrate these equations of motion, supplemented with suitable initial condition, by the fourth-order Runge-Kutta method due to Gill.[24] The iteration step size t_{step} (in units of t_0) was chosen after the tests involving the conservation of lengths of the spin vectors and behavior under time reversal. Obviously the time evolution of each of the spin configurations in the MD has to be terminated after a finite duration t_{max}. This produces an intrinsic linewidth in the computed dynamic structure function $S(\mathbf{q},\omega)$ of the order of h/t_{max}. Thus taking into account the relevant resolution width, as is of experimental interest, we fix t_{max} again in units of t_0. In each dynamical run we store $\mathbf{S}_q(t)$'s (for the q's of interest) and real space spin configurations $\mathbf{S}_i(t)$'s at some regular intervals of time Δt_s, starting from the initial condition at $t=0$. We use these to calculate various time-dependent correlation functions. So the operational definitions for calculating these quantities of interest become

$$C(0,t)=\frac{1}{N_cN(M-p)}\left[\sum_{c=1}^{N_c}\sum_{i=1}^{N}\sum_{m=0}^{M-p}[\mathbf{S}_i(m\Delta t_S)]_{(c)}\cdot[\mathbf{S}_i((p+m)\Delta t_S)]_{(c)}\right],\tag{3.21}$$

$$C_q(t)=\frac{1}{N_c(M-p)}\left[\sum_{c=1}^{N_c}\sum_{m=0}^{M-p}[\mathbf{S}_q(m\Delta t_S)]_{(c)}\cdot[\mathbf{S}_{-q}((p+m)\Delta t_S)]_{(c)}\right],\tag{3.22}$$

where $t_{\text{max}}=M\Delta t_S$ and $t=p\Delta t_S$; c denotes a MD sample chosen for a dynamical run, i denotes a lattice site, N_c is the total number of MD samples, and N is the total number of lattice sites. We calculate $C_q(t)$ for $t=0$ to $t_{\text{max}}/2$, since the calculated $C_q(t)$'s for $t>t_{\text{max}}/2$ have much less accuracy. So $C_q(p\Delta t_S)$ is stored for $p=0,1,\ldots,M/2$. Now the trajectory in a MD simulation depends upon the values of various conserved parameters as well as upon the detailed structure of the spin configuration of the initial state. However, for a sufficiently long time evolution in the MD (viz., time of the order of e^N) the results for various dynamical quantities become independent of the initial state when the initial state is chosen to be any state in a MD trajectory. But since the MD calculations in practice involve time evolutions of much shorter duration, this initial condition independence of the magnitude of various dynamical quantities, i.e., "ergodicity" (as used in the literature for the time series analysis) does not hold. To reduce the unwanted fluctuations in the estimates of the dynamical quantities because of this fact, we have modified the definitions (3.21) and (3.22) by replacing $t_{\text{max}}-t$ with t_{max}, i.e., $(M-p)$ with M in the denominator, as is very often done in the finite-time series problems.[25] This method is known to give lesser mean square error in the estimates in real time domain compared to the old definition with $t_{\text{max}}-t$ in the denominator, and also does not lead to unwanted humps in the Fourier spectra unlike the former definition.[25] Thus this method is preferred. We have used these modified equations to calculate $S(\mathbf{q},\omega)$ and $C(0,t)$ and have compared them with the results obtained with the unmodified definitions.

We call, for simplicity, the modified definition the definition A and the unmodified one the definition B. We illustrate the results of our calculations, done using these two definitions, for $S(\mathbf{q},\omega)$ and for $C(0,t)$ in Tables IV and V, respectively, in Sec. IV. We indeed find that definition A gives lesser fluctuations than definition B in the estimates for both $S(\mathbf{q},\omega)$ and $C(0,t)$.

It may be worthwhile to point out that though MD is a purely deterministic dynamics, for a system with a very large number of interacting spins N, as is the case here, the trajectory of the system point in the $3N$-dimensional spin configuration space looks like that due to a stochastic motion. This fact enables us to look upon the MD as a time series phenomenon.

We also noted the fact that we are dealing with a very small number of MD samples, viz. $N_c=10$. Thus it is important to examine whether these MD samples can give a reliable estimate for the ensemble averages of various dynamical quantities. For these we compared the estimates of the static properties, viz. $C_q(0)$'s from the MC and from the MD for all the allowed q vectors along the $\langle 111\rangle$ direction. We found that the MD and the MC estimates are quite close to each other and differ by an amount less than the difference in the MC estimates themselves in two different MC simulations. Since the MC estimate of $C_q(0)$ is quite reliable, as mentioned earlier, we feel that 10 MD samples, chosen at 1000 MC steps/spin difference of the MC ages, can give satisfactory estimates of the ensemble averages of various quantities of interest.

Now we calculate $S(\mathbf{q},\omega)$ by using the definition

$$S(\mathbf{q},\omega)=\frac{1}{\pi}\int_0^{t_{max}/2}\mathrm{Re}[C_\mathbf{q}(t)]R(t)\cos(\omega t)dt \qquad (3.23)$$

[we only use the real part of $C_\mathbf{q}(t)$ in the above expression] where t_{max} is the time of evolution in MD, $R(t)$ is the Tukey spectral smoothing function;

$$R(t)=0.5\left[1+\cos\left[\frac{2\pi t}{t_{max}}\right]\right] \quad \text{for } |t|\le t_{max}/2$$

and $R(t)=0$ for $|t|>t_{max}/2$.

$R(t)$ is used in the expression for $S(\mathbf{q},\omega)$ to reduce the spectral distortion produced by the finite time truncation of the time evolution in the MD. We evaluate the above integral in the expression for $S(\mathbf{q},\omega)$ by the Simpson's quadrature formula with the iteration size being equal to Δt_S. We have also tried another method due to Takahashi[23] to evaluate the time integral. In this method one performs summation over the MD data stored at the finite-time intervals and also uses the periodic boundary condition in time. We found that the tail intensities decay much faster with the energy in the first method compared to the second method but the positions of the peaks are more or less the same in both the methods in the constant $\mathbf{q}$ scans of $S(\mathbf{q},\omega)$. However, we feel that the method involving the Simpson's rule is the more logical one and we present almost all our major and important results in this paper only using this method. The resolution width of our calculation is equal to the full width at half maximum (FWHM) of the Fourier transform of $R(t)$. This can be shown to be exactly equal to $2h/t_{max}$ (see Appendix D). For calculating $\mathbf{S}_\mathbf{q}(t)$ and hence $C_\mathbf{q}(t)$ we used the fast Fourier transform technique.

Since our calculation is a statistical one, it involves sampling from the ensemble configurations, so to speak, we also need to have an estimate of the error bars in the estimates of various quantities of interest like $C(0,t)$, $C_\mathbf{q}(t)$, $S(\mathbf{q},\omega)$, etc. But this is not a very simple task. We in fact performed two independent MCMD simulations involving 10 samples each, on a $10\times10\times10$ lattice containing 4000 spins at the temperature $2.0T_c$. We then compared the estimates of $C_\mathbf{q}(t)$ for two values of q along $\langle 111\rangle$, viz. $q=q_{min}>0$ and $q=q_{ZB}$, from these two simulations (q_{ZB} denotes the wave vector at the zone boundary). We display the results for $C_\mathbf{q}(t)$ from the first set of 10 samples, from the second set of 10 samples, and from the grand set comprising all these 20 samples for $q=q_{min}$, in Fig. 1(a). The corresponding results for difference in the estimates of $C_\mathbf{q}(t)$ from the two simulations is always much less than the rms fluctuation in $C_\mathbf{q}(t)$ obtained from any one simulation [see Figs. 1(a) and 1(c)]. We found the same feature also in the spectral function $S(\mathbf{q},\omega)$. In fact, we found that we can safely take 50% of the rms fluctuation value in $S(\mathbf{q},\omega)$, obtained from any one simulation, as the corresponding magnitude of the error in $S(\mathbf{q},\omega)$. We also tried another method originally used by Shastry in the iron problem.[9] In this method one estimates $C_\mathbf{q}(t)$ by using the equation

$$\langle C_\mathbf{q}(t)\rangle=\left\langle\frac{C_\mathbf{q}(t)}{C_\mathbf{q}(0)}\right\rangle_{MD}\langle C_\mathbf{q}(0)\rangle_{MC} , \qquad (3.24)$$

where $\langle\ \rangle$ denotes here the estimate for the ensemble average and $\langle\ \rangle_{MD}$ is calculated using an equation of the type (3.22) with the modified denominator, as mentioned earlier. We display the results for $\langle C_\mathbf{q}(t)\rangle$ calculated using this decoupled definition from the first set, from the second set, and from the grand set for $q=q_{min}$ in Fig. 1(b). The corresponding results for $q=q_{ZB}$ are displayed in Fig. 1(d). We found that the estimates given by this method are quite close to the corresponding estimates by our direct and new method, described earlier [see Figs. 1(a)–1(d)]. We also found that the rms fluctuations in $S(\mathbf{q},\omega)$ obtained from the 10 MD samples in Shastry's method are fairly close to the corresponding errors in $S(\mathbf{q},\omega)$ obtained by our new method for all $\mathbf{q}\ne0$. It should be pointed out that Shastry quoted the rms fluctuation value (obtained from the 10 MD samples in his method) itself as the magnitude of the error. Shastry's method gives less rms fluctuation compared to our new method because $C_\mathbf{q}(t)/C_\mathbf{q}(0)$ is a more slowly varying function of the ensemble configurations than $C_\mathbf{q}(t)$. Thus on the whole, we feel that practically either of the two methods is equally good, but in this paper we present the results of the calculations done by the new method only. The deviations of the estimates for various quantities in the finite size system, as used in our calculations, from the corresponding estimates in the thermodynamic limit are expected to be of the order of $1/\sqrt{N}$, which comes to about 2% in our case. This is much less than the error arising out of the finite number of the MD samples, etc., which is indicated as the error bar in our calculation.

The calculation of the static properties and checking the reliability of the estimates from the MD samples, mentioned earlier, were also done using the simulation results from a $10\times10\times10$ lattice at the temperature $2.0T_c$.

For the calculation of the spin autocorrelation function we could store $\mathbf{S}_i(t)$'s corresponding to only 400 spins, because of the storage space restrictions. We chose these 400 lattice sites randomly, with equal probability for every site in the whole finite lattice to be chosen and with the condition that no sites were to be chosen more than once. We also checked the reliability of the estimate for the autocorrelation function from the set of 400 spins, by partitioning this set into two smaller sets of 200 spins each by means of the random selections, and then comparing the estimates obtained from the grand set and the two smaller sets, respectively. This exercise was done on a $10\times10\times10$ lattice at the temperature $2.0T_c$. We found that the three estimates are very close to each other.

We finally performed the simulations on a bigger lattice, viz. $12\times12\times12$ containing 6912 spins at two different temperatures, viz. $2.0T_c$ and $1.68T_c$. This was the largest lattice we could perform simulation on, within the allowed resources of the computer, to reduce the finite-size effects. These two temperatures were so chosen that we could compare our simulation results with Mook's experimental results for $2.0T_c$ and Böni and Shirane's results for $1.68T_c$. We probed all the three principal directions, viz. $\langle 111\rangle$, $\langle 110\rangle$, and $\langle 100\rangle$ in our simulation and calculated $S(\mathbf{q},\omega)$ by our new method. We also calculated the spin autocorrelation function at those two temperatures. We compared the results for

$S(\mathbf{q},\omega)$ obtained from the simulation on this bigger lattice $(12\times12\times12)$ with the experimental results and also with the results of the YS theory and of Lindgard's theory. Since, for a finite system, we have only discrete values of q, sometimes the comparisons were made for the closest possible q value allowed by the box-quantization scheme.

The values of J_1 and J_2, used in our calculation, are those extracted from the experimentally obtained spin wave dispersion curve at low temperature in the ordered phase.[26] The value of T_c used in this calculation is the experimental T_c. This value of T_c agrees very well with that obtained by the high-temperature series expansion

results for the classical Heisenberg model.[26,27] It must, however, be noted that the value of T_c obtained from the YS calculation is slightly different from that used in our calculation. For comparing with our results for the static and the dynamic properties, we have calculated the corresponding quantities using the YS theory at the same values of T/T_c ratios, viz. 1.68 and 2.0. Lindgard's theory also gives slightly different values of T_c. We have again compared our results with those of Lindgard for the same value of T/T_c, viz. 2.0.

All the simulation work reported in this paper was done on a Cyber 170/730 computer. Each dynamical run takes about 2 h of CPU time. The resolution width of
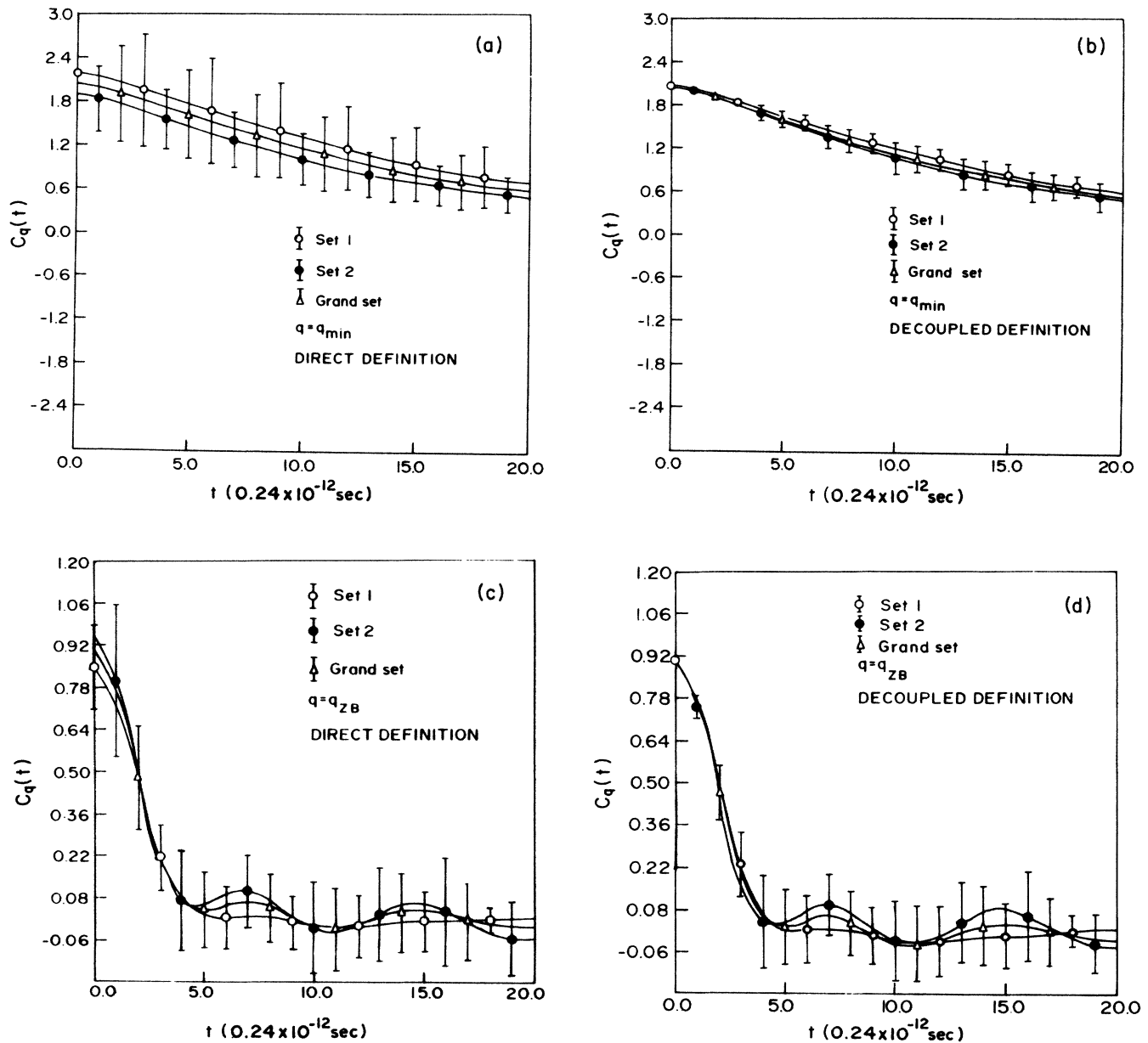

FIG. 1. $C_q(t)$ vs t plots for two values of q along $\langle 111\rangle$, from the MCMD calculation at the temperature $2.0T_c$ using a $10\times10\times10$ lattice, with the direct definition and Shastry's decoupled definition: (a) $q=q_{min}>0$ and direct definition, (b) $q=q_{min}>0$ and Shastry's decoupled definition, (c) $q=q_{ZB}$ and direct definition, (d) $q=q_{ZB}$ and Shastry's decoupled definition.

our calculation is about the same as that in Böni and Shirane's experiments, viz. the half width at half maximum (HWHM) equal to 0.43 meV. For comparison with our results, we have convoluted the YS results with the same resolution function of the same width as used in our calculation. Mook does not quote the resolution width in his experiments. We have not convoluted the $S(\mathbf{q},\omega)$ results of Mook and of Lindgard with any resolution function and displayed only the corresponding bare results in our previous figures.

Since the reported results of Böni and Shirane, of Mook, and also of Lindgard for $S(\mathbf{q},\omega)$ are not in the absolute scales, we have normalized them suitably for comparing with our results. The scheme used for normalization was as follows: at the temperature $2.0T_c$ for $q \equiv 0.5q_{ZB}$ along $\langle 111 \rangle$, the normalization constant was so chosen that our results and Mook's results coincide at the energy value of 0.82 meV; at the same temperature for $q \equiv q_{ZB}$ along $\langle 111 \rangle$, the constant was fixed by making our results and Mook's results coincide at the energy value of 0.57 meV. These normalization constants were used for comparing our results with the results of Mook and of Lindgard. We have multiplied the results of Mook and of Lindgard with these normalization constants. At the temperature $1.68T_c$ for all four q values of interest, we have determined the normalization constants by matching our results for $\langle 111 \rangle$ and Böni and Shirane's results for the powder at $\omega = 0$. These normalization constants were used to scale Böni and Shirane's results for comparing with ours. It may be pointed out that we could have chosen a different and probably better normalization scheme by which we could have brought the curves of Böni and Shirane, of Mook, and of Lindgard much closer to our curves from the MCMD. All the curves from the convoluted YS are to be multiplied by a factor of 3, to bring them on absolute scale.

IV. RESULTS

In this section we give all our important results, for both the static and the dynamic properties, and compare them with those from the other theoretical and experimental approaches at the appropriate places. The constants we used are

$$J_1 = 1.204 \text{ K}, \quad J_2 = 0.310 \text{ K}, \quad T_c = 69.15 \text{ K}, \quad a = 5.12 \text{ Å},$$

$$t_0 = 1.6 \times 10^{-12} \text{ sec}, \quad t_{\text{step}} = 0.015 t_0.$$

TABLE I. Monte Carlo estimates of the static spin-spin correlation function in the q space C_q (for q along $\langle 111 \rangle$) at $T = 2.0T_c$.

q/q_{ZB}	$(C_q)_{av}$	$(C_q)_{rmsf}$	$(C_q)_{rmsf}/(C_q)_{av}$
0.0	2.4669	2.1258	0.8617
0.2	2.0704	1.2028	0.5810
0.4	1.5106	0.8955	0.5928
0.6	1.1430	0.6725	0.5884
0.8	0.9429	0.5160	0.5472
1.0	0.9036	0.7325	0.8106

TABLE II. Ritchie-Fisher (RF) functional fit for $(C_q)_{av}$ (with q along $\langle 111 \rangle$) at $T = 2.0T_c$. The value of $C_{q=0}$, mentioned here, is that calculated using the best-fit values of the RF parameters.

$\alpha = 1.6968$
$\beta = 0.6831$
$C_{q=0} = 2.4630$
$\xi = 1.37$ Å

For convenience, we hereafter refer to $C_q(0)$ as C_q and $C(r,0)$ as $C(r)$. The true estimates for C_q, $C(r)$, and $C(0,t)$ are obtained by multiplying them with the factor $S(S+1)$ which is equal to 15.75 in this case. This also implies multiplication of the value for α by the same factor.

A. Static properties (at $T = 2.0T_c$)

We display in Tables I–III the results for various static properties from our MC calculations and also give the static results of YS and of Lindgard's calculations for comparison. In Table I we present the results for the MC estimates of C_q (both average and rms fluctuation) for q along the $\langle 111 \rangle$ direction. In Table II we give the appropriate parameters obtained by fitting the estimates of $(C_q)_{av}$ to the Ritchie-Fisher (RF) functional form. In Table III we display the results for $C(r)$ from (i) our direct MC estimates, (ii) the Fourier transformation of the RF fitted form of $(C_q)_{av}$ in our MC calculations, (iii) the calculations of YS, and also (iv) the calculations of Lindgard. As mentioned earlier, the MC results displayed here are those obtained with the $10 \times 10 \times 10$ lattice.

B. Dynamic properties

We first display the fact that definition A gives lesser absolute fluctuations compared to definition B in the estimates for $S(\mathbf{q},\omega)$ as well as for $C(0,t)$ in almost all the cases, in Tables IV and V, respectively. The results for $S(\mathbf{q},\omega)$ used in Table IV correspond to $q \equiv q_{ZB}$ along $\langle 111 \rangle$ and have been obtained using Takahashi's approach. These results in Table IV as well as the results for $C(0,t)$ displayed in Table V are from our simulations on a $10 \times 10 \times 10$ lattice at the temperature $2.0T_c$. Then in the separate figures we display the $S(\mathbf{q},\omega)$ results for various values of q and also our results for the spin autocorrelation function corresponding to the two temperatures $1.68T_c$ and $2.0T_c$. The $S(\mathbf{q},\omega)$ results displayed include our MCMD results, as well as the results from other theoretical approaches and experiments. We also give $C_q(t)$ versus t plots corresponding to the two definitions, viz. the direct definition and the decoupled definition for the two values of q, as mentioned earlier. All the results presented in the figures have been obtained by using $1/t_{max}$ definition, i.e., definition A only.

TABLE III. Results for the static spin-spin correlation function in the real space $C(r)$ at $T = 2.0T_c$.

Neighbor-shell number	Distance (in units of a)	$C(r)$ (MC)	$C(r)$ (RF)	$C(r)$ (YS)	$C(r)$ (Lindgard)
1	$1/\sqrt{2}$	0.0606	0.0766	0.0643	0.0702
2	1	0.0246	0.0316	0.0062	0.0298
3	$\sqrt{3/2}$	0.0091	0.0139	0.0008	
4	$\sqrt{2}$	0.0055	0.0097	0.0001	

$(\xi)_{RF} = 1.37$ Å, $(\xi)_{YS} = 2.00$ Å, $(\xi)_{LINDGARD} = 1.20$ Å

V. DISCUSSION

Figures 2(a)–2(d) contain the $S(\mathbf{q},\omega)$ results at the temperature $1.68T_c$ for $q \simeq 0.4$ Å^{-1}, $q \simeq 0.6$ Å^{-1}, $q \simeq 0.8$ Å^{-1}, and $q \simeq 1.0$ Å^{-1}, respectively. The theoretical results are for the $\langle 111 \rangle$ direction, whereas the experimental results are for the powder form. Figures 3(a), 3(b), and 3(c) contain the $S(\mathbf{q},\omega)$ results for $\mathbf{q}$ along the $\langle 111 \rangle$ direction at the temperature $2.0T_c$ corresponding to the $\mathbf{q}$ values of $0.5q_{ZB}$, $0.8q_{ZB}$, and q_{ZB}, respectively.

Looking at Figs. 2(a)–2(d) and also at 3(a), 3(b), and 3(c), we find that our results for $S(\mathbf{q},\omega)$ agree qualitatively with the results of the recent experiments performed by Böni and Shirane as well as with the previous measurements by Mook. However, the quantitative features of our results are closer to those of the observations of Böni and Shirane than to those of the observations of Mook. Turning to the comparison of our results with the results of other theoretical approaches, from the above-mentioned figures we find that our results show features which are very similar to those from the YS calculations. The agreement between our results and those of Lindgard's is much less. Also, from those same figures mentioned above, we see that our calculated $S(\mathbf{q},\omega)$ shows distinct qualitative features in the low-q regime and in the high-q regime. When plotted in the constant $\mathbf{q}$ scans as a function of ω, our results for $S(\mathbf{q},\omega)$ show a peak only at $\omega = 0$ for low values of q, indicating purely

diffusive behavior [see Figs. 2(a), 2(b), and 3(a)]. For the q values in the upper half of the magnetic zone, in particular close to the zone boundary, our calculated $S(\mathbf{q},\omega)$ shows three-peak structures consisting of a central peak and two peaks or shoulders at finite values of ω (both positive and negative), displaying the existence of damped propagating modes [see Figs. 2(c), 2(d), 3(b), and 3(c)]. In the propagating regime we seem to get more intensity for the central peak than for the peaks at finite values of ω, at both the temperatures, as observed in Böni and Shirane's experiments and also in the YS calculations. We also find from the comparison of our results for $S(\mathbf{q},\omega)$ for $\mathbf{q}$ along the three principal directions, with the same value of $|\mathbf{q}|$ (approximately), that the isotropy is fairly good, as claimed by Böni and Shirane, if we take into account the error bars and the resolution width (HWHM) in our MCMD calculation. The convoluted YS results also support this, when we take into consideration the resolution width. For brevity we have only displayed the $S(\mathbf{q},\omega)$ results from the MCMD and from the convoluted YS, obtained at $T = 1.68T_c$ for $\mathbf{q}$ along the three principal directions with $|\mathbf{q}|$ approximately equal to the value for q_{ZB} corresponding to $\langle 111 \rangle$, to establish our claim for the isotropy. The results corresponding to the $\langle 111 \rangle$, $\langle 110 \rangle$, and $\langle 100 \rangle$ directions are displayed in Figs. 2(d), 4(a), and 4(b), respectively. The structure seen in our calculated $S(\mathbf{q},\omega)$ in the constant-q plots (from the various figures mentioned earlier) also gets qualitative support

TABLE IV. Monte Carlo–molecular-dynamics results for the dynamic structure function $S(\mathbf{q},\omega)$ with two definitions.

$\hbar\omega$ (in units of 0.43 meV)	$S(\mathbf{q},\omega)/\hbar$ (def. A) (10^{-2} meV^{-1})	rmsf (def. A) (10^{-2} meV^{-1})	$S(\mathbf{q},\omega)/\hbar$ (def. B) (10^{-2} meV^{-1})	rmsf (def. B) (10^{-2} meV^{-1})
1.0	0.3187	0.1150	0.3277	0.1321
2.0	0.3158	0.0808	0.3250	0.0866
3.0	0.2931	0.0486	0.3006	0.0535
4.0	0.2529	0.0545	0.2560	0.0620
5.0	0.2132	0.0578	0.2134	0.0636
6.0	0.1808	0.0402	0.1813	0.0411
7.0	0.1464	0.0303	0.1454	0.0315
8.0	0.1120	0.0225	0.1084	0.0237
9.0	0.0895	0.0131	0.0849	0.0119
10.0	0.0796	0.0133	0.0760	0.0133

TABLE V. Monte Carlo–molecular-dynamics results for spin autocorrelation function $C(0,t)$ with two definitions.

t (in units of t_0)	$C(0,t)$ (def. A)	rmsf (def. A)	$C(0,t)$ (def. B)	rmsf (def. B)
0.0	1.0000	6.2×10^{-8}	1.0000	6.2×10^{-8}
0.15	0.8612	0.0045	0.8828	0.0046
0.30	0.5790	0.0124	0.6087	0.0130
0.45	0.3098	0.0148	0.3342	0.0160
0.60	0.1468	0.0104	0.1627	0.0115
0.75	0.0856	0.0070	0.0975	0.0080
0.90	0.0745	0.0082	0.0872	0.0096
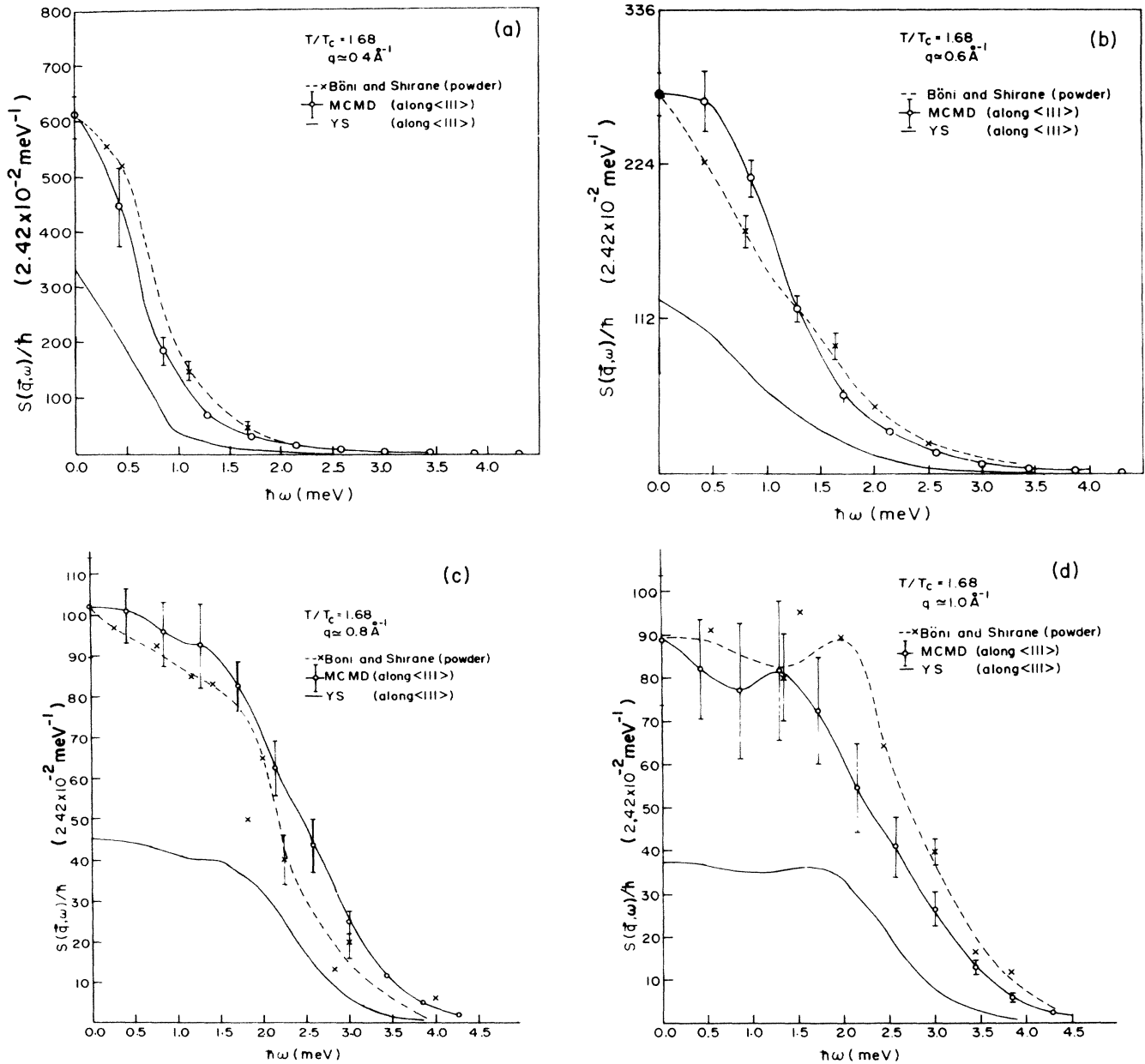
FIG. 2. $S(\mathbf{q},\omega)$ results from the MCMD, YS, and Böni and Shirane at the temperature $1.68T_c$ for four values of q. The results from the MCMD and YS are for $\langle 111 \rangle$, whereas the results of Böni and Shirane are for the powder. As mentioned earlier in the text, the YS curves are to be multiplied by a factor of 3. (a) $q \simeq 0.4$ Å^{-1}, (b) $q \simeq 0.6$ Å^{-1}, (c) $q \simeq 0.8$ Å^{-1}, (d) $q \simeq 1.0$ Å^{-1}, i.e., $q \simeq q_{\rm ZB}$ along $\langle 111 \rangle$.

from the results we obtained in the $C_q(t)$ versus t plots displayed in Figs. 1(a)–1(d). The general feature seen in our $S(q,\omega)$ results in the propagating region, viz. the softening of the modes, the reduction in the intensities for the peaks at finite frequencies, and also the broadening of these peaks, with increase in temperature [see Figs. 2(c), 2(d), 3(b), and 3(c)] are as well seen in the experiments performed by Böni and Shirane, by Mook, and also occur in the results of YS and of Lindgard. It must, however, be pointed out that the peak positions in the propagating region in our calculation are very close to those in Böni and Shirane's experiments, in the YS calculations, and also in Lindgard's calculations but are slightly different (in fact shifted towards lesser value) from those obtained in Mook's experiments, as seen from Figs. 2(c), 2(d), 3(b), and 3(c). Our results also exhibit more intensity in the low-q scans compared to the high-q scans, in agreement with the results of Böni and Shirane, YS, Mook, and Lindgard [see Figs. 2(a)–2(d), 3(a), 3(b), and 3(c)]. This is in accordance with the fact that the system is heading to-
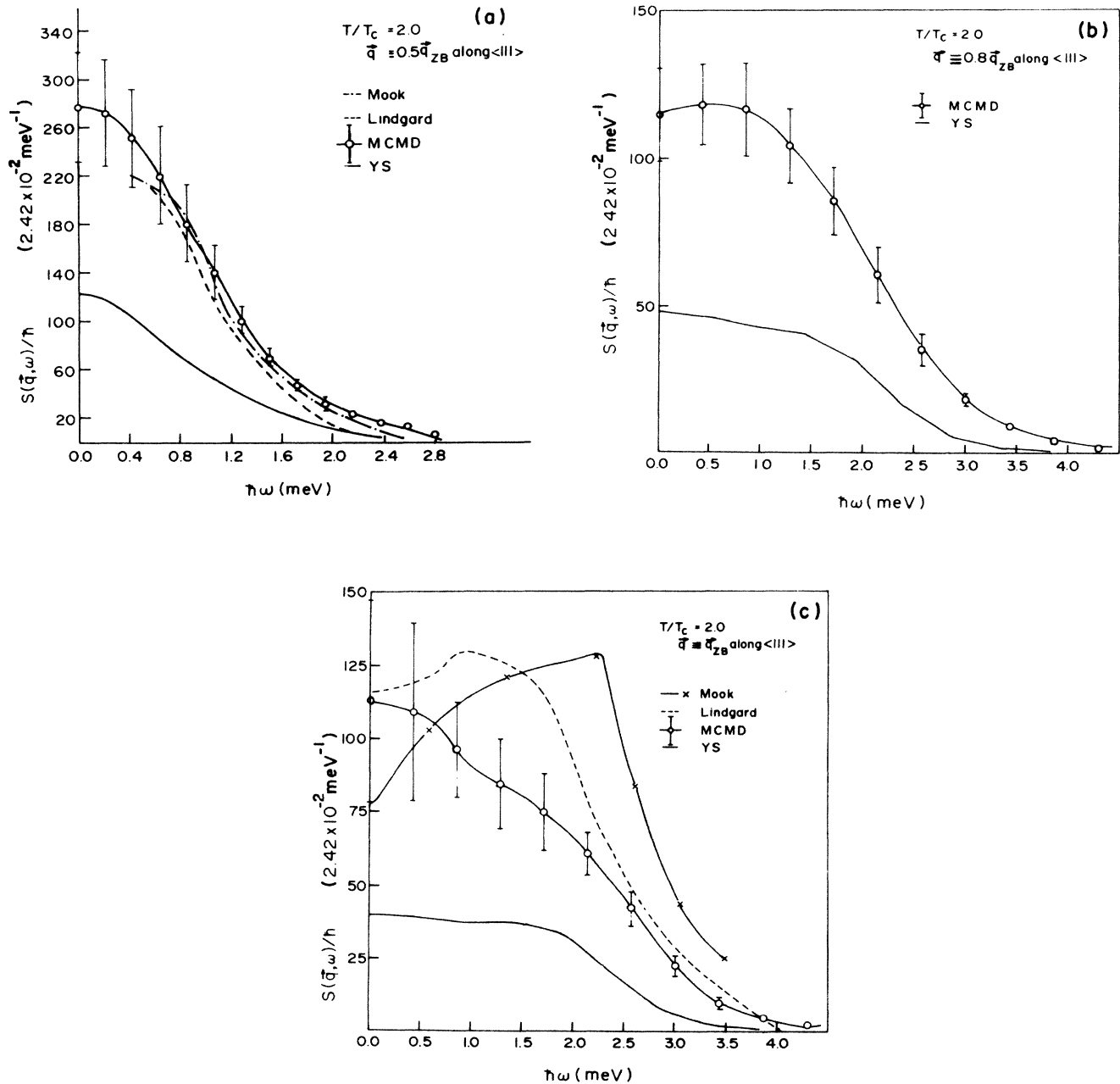

FIG. 3. $S(q,\omega)$ results from the MCMD, YS, Lindgard, and Mook for three values of q along $\langle 111 \rangle$ at the temperature $2.0T_c$ (the YS curves are to be multiplied by a factor of 3): (a) $q \equiv 0.5q_{ZB}$; MCMD, YS, Lindgard, and Mook, (b) $q \equiv 0.8q_{ZB}$; MCMD and YS, (c) $q \equiv q_{ZB}$; MCMD, YS, Lindgard, and Mook.

wards a ferromagnetic instability.

We see from Figs. 2(a)–2(d) that the neutron scattering results of Böni and Shirane for $S(q,\omega)$ for the powder form of EuO agree quite well with our results for $S(q,\omega)$ for the $\langle 111 \rangle$ direction, both qualitatively and quantitatively for all four values of q probed. We also find a good agreement with the convoluted YS results for the $\langle 111 \rangle$ direction. The values of q at which Böni and Shirane observe propagating modes, our calculations also show the

same. Moreover, our predicted positions of the peaks or the shoulders in the $S(q,\omega)$ curves are very close to those from Böni and Shirane's experimental results and to those from the results of the convoluted YS, within the resolution width (HWHM) and the error bars.

Our results for the spin autocorrelation function at the temperatures $2.0T_c$ and $1.68T_c$ are displayed in Figs. 5(a) and 5(b), respectively. From these figures we see that the spin autocorrelation function shows a purely diffusive be-
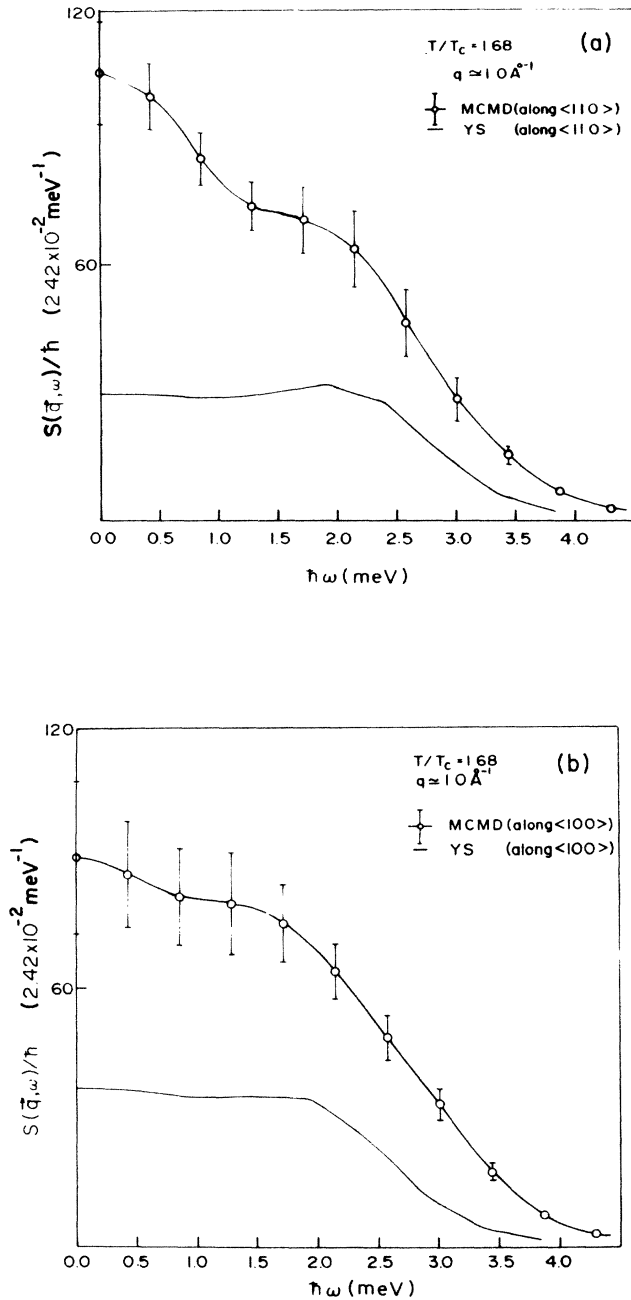

FIG. 4. $S(q,\omega)$ results from the MCMD and YS at the temperature $1.68T_c$ for q along $\langle 110 \rangle$ and $\langle 100 \rangle$ with $|q| \simeq 1.0$ Å^{-1} (the YS curves are to be multiplied by a factor of 3): (a) $\langle 110 \rangle$; (b) $\langle 100 \rangle$.
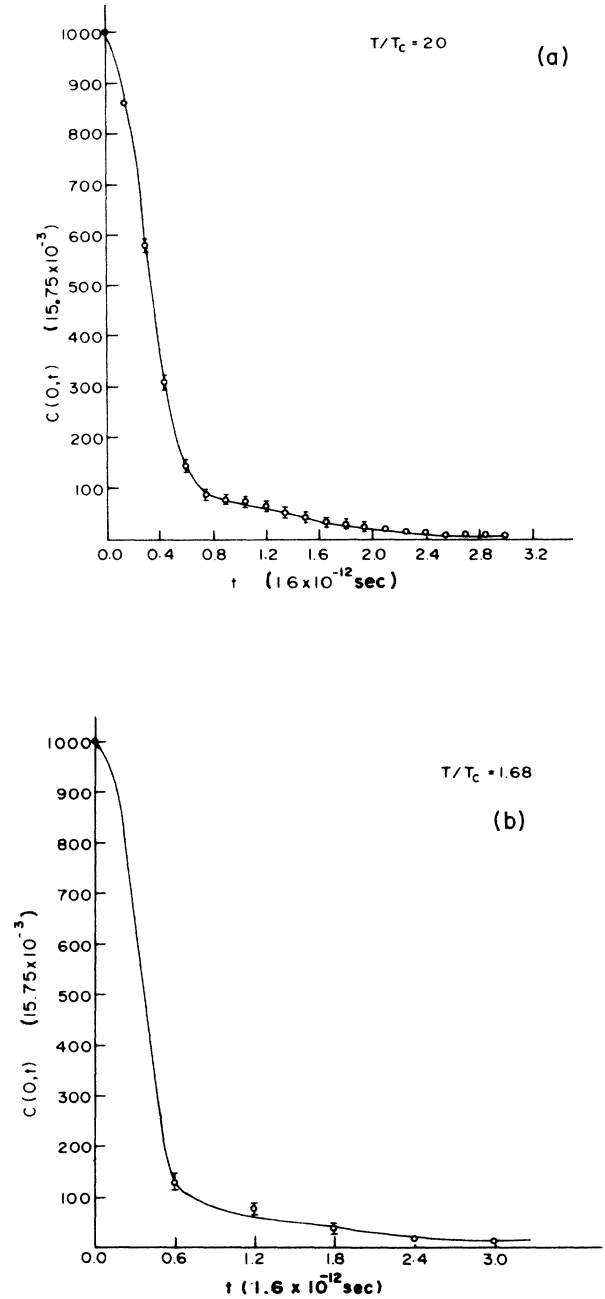
FIG. 5. The spin autocorrelation function from the MCMD for two different temperatures: (a) $2.0T_c$ with $10 \times 10 \times 10$ lattice, (b) $1.68T_c$ with $12 \times 12 \times 12$ lattice.

havior as a function of time at both the temperatures. The result seems to be less sensitive to the temperature and also to the lattice size, compared to the results for $S(\mathbf{q},\omega)$. As mentioned earlier, there are still no experimental results for the spin autocorrelation function of EuO.

From Table III containing some of the static results, we see clearly that the qualitative features of our results agree quite well with those of the results of YS and of the results of Lindgard, but in the quantitative estimates our results seem to be closer to those of Lindgard than to those of YS. As mentioned earlier, our estimates for $C_{\mathbf{q}}(0)$ at the temperature $2.0T_c$ from the Monte Carlo calculations and from the molecular dynamics calculations are pretty close to each other. This shows the reliability and the consistency of our overall calculation.

The detailed comparison of our results for the static and the dynamic properties with those from the two other theoretical approaches and the two different experiments, seem to bring out certain interesting features. The good agreement between our results and Böni and Shirane's results show that the spin dynamics of EuO in the paramagnetic phase can be very well explained by the Heisenberg model with ferromagnetic interactions ranging up to the second-neighbor shell. Since this model also gives a very good estimate of T_c, we can say that the Heisenberg model provides a very good description of both the static and the dynamic properties of the paramagnetic EuO. The predictions of the YS theory regarding the dynamic properties of the Heisenberg model, appropriate to EuO, seem to be quite good. This also reflects the validity of the three-pole approximation of Lovesey and Meserve in this particular case. For low values of q, the intensities from the YS calculation give more weightage to low ω, whereas in the high-q regime the intensities give higher weightage to the higher values of ω. However, the two-pole approximation, as used by Lindgard, seems to be a bad approximation for the spin dynamics in this case. Surprisingly enough, the predictions of Lindgard's theory for the static properties seem to be better than those of the YS theory for the same, in this particular case. This seems to imply that the self-consistency condition used in Lindgard's theory to calculate the static quantities from the dynamic quantities, works pretty well in this case. The spherical model approximation used by YS seems to be not so good in this case. In any case, both the theories in agreement with our results, show that propagating modes can exist even in the absence of any giant short-range ordering in the paramagnetic phase of the Heisenberg model. In fact, we found from our calculations that the correlation length ξ is much less than the wavelengths corresponding to the various values of q at which we get the pseudopropagating modes. This is supported by the other two theories also. Thus we feel that the existence of the pseudopropagating mode in the paramagnetic phase of the Heisenberg model primarily depends upon the equations of motion. This explains why experimentally one has observed such a strong dependence of the nature of the collective excitations in the paramagnetic phase of the Heisenberg systems, on various factors like the type and

the range of the exchange interactions, the type of the lattice, the value of the spin of the magnetic atoms, etc. We also feel that the reason for the occurrence of the three peaks in the propagating regime in the paramagnetic phase is quite different from that for the three-peak structure observed in the ordered phase. In the ordered phase the peaks at the finite frequencies, i.e., the spin wave peaks occur because of the existence of oscillatory (slightly damped) solutions for the equation of motion of the dynamic correlation function for the transverse components of the spins. The quasielastic central peak arises mainly due to the almost steady (slightly temporally damped) correlation between the longitudinal components of the spins. However, in the paramagnetic phase, the distinction between the longitudinal and the transverse components vanishes completely. Thus there is a complete isotropy in the equations of motion. So the three-peak structure for $S(\mathbf{q},\omega)$ observed in the paramagnetic phase is due to the equation of motion of the correlation function corresponding to any component of the spin. Thus it is clear that in the paramagnetic phase, the two-spin dynamic correlation function in $\mathbf{q}$ space, for any spin component, for $\mathbf{q}$ close to the zone boundary, has a temporal evolution which gives rise to this structure. However, for the low values of q, the temporal evolution of this correlation function is purely diffusive and produces only a central peak in the Fourier spectrum. These features remain intact even for temperatures very close to T_c in the paramagnetic phase, as is seen in Böni and Shirane's experiment.

From the equation of motion approach using the microscopic theory, we know that the temporal evolution of the two-spin dynamic correlation function in $\mathbf{q}$ space is governed by various higher-order dynamic correlation functions which have nontrivial temperature and $\mathbf{q}$ dependence. This leads to the observed $\mathbf{q}$ dependence of the qualitative features of $S(\mathbf{q},\omega)$ in the paramagnetic phase. For the spin dynamics, the static properties seem to play the most crucial role only in bringing about a qualitative change in the nature of the collective excitations, as the system undergoes a magnetic phase transition. However, in the paramagnetic phase, the static properties only affect certain quantitative features of $S(\mathbf{q},\omega)$, viz. the peak position, the width, etc. The most direct way of seeing the roles of the short-range order and of the static properties in determining the nature of the spin dynamics, is to follow the philosophy of the MCMD technique, as described earlier. The static properties come in the form of the initial conditions, i.e., the spin configurations of the MD samples.

APPENDIX A: WINDSOR'S DETAILED BALANCE FACTOR

The central point in Windsor's[19] prescription is that in time domain, the classical correlation function is equated

to the real part of the quantum correlation function. This is essentially an Ansatz and is quite popular in the molecular dynamics studies. For a centrosymmetric system, this ansatz leads to the relation between $S_{QM}(\mathbf{q},\omega)$ and $S_{cl}(\mathbf{q},\omega)$, as suggested by Windsor. To see it clearly, we first make use of the equations involving the linear response functions and the correlation functions, as occurs in the fluctuation-dissipation theorem:

$$\langle \mathbf{S_q}(0)\cdot\mathbf{S_{-q}}(t)\rangle_{QM}= \int_{-\infty}^{+\infty} \frac{d\omega}{\pi} e^{i\omega t}\frac{1}{1-e^{-\hbar\omega\beta}}\chi''_{QM}(\mathbf{q},\omega) , \tag{A1}$$

$$\langle \mathbf{S_{-q}}(t)\cdot\mathbf{S_q}(0)\rangle_{QM}= \int_{-\infty}^{+\infty} \frac{d\omega}{\pi} e^{i\omega t}\frac{1}{e^{\hbar\omega\beta}-1}\chi''_{QM}(\mathbf{q},\omega) . \tag{A2}$$

Thus

$$\langle \tfrac{1}{2}\{\mathbf{S_q}(0),\mathbf{S_{-q}}(t)\}\rangle_{QM}$$
$$= \int_{-\infty}^{+\infty} \frac{d\omega}{2\pi} e^{i\omega t}\coth(\hbar\omega\beta/2)\chi''_{QM}(\mathbf{q},\omega) . \tag{A3}$$

Now by Windsor's prescription

$$\langle \mathbf{S_q}(0)\cdot\mathbf{S_{-q}}(t)\rangle_{cl}\simeq\tfrac{1}{2}\langle\{\mathbf{S_q}(0),\mathbf{S_{-q}}(t)\}\rangle_{QM} . \tag{A4}$$

This leads to

$$S_{cl}(\mathbf{q},\omega)= \frac{1}{2\pi}\coth\left[\frac{\hbar\omega\beta}{2}\right]\chi''_{QM}(\mathbf{q},\omega)$$
$$=\tfrac{1}{2}\coth\left[\frac{\hbar\omega\beta}{2}\right](1-e^{-\hbar\omega\beta})\cdot S_{QM}(\mathbf{q},\omega) , \tag{A5}$$

$$S_{QM}(\mathbf{q},\omega)= \frac{2}{1+e^{-\hbar\omega\beta}}S_{cl}(\mathbf{q},\omega) . \tag{A6}$$

APPENDIX B: RATIO OF $(C_q)_{rmsf}$ TO $(C_q)_{av}$ IN THERMAL EQUILIBRIUM

By the central limit theorem, for a system in the paramagnetic phase, we have

$$P(\mathbf{M})=\mathcal{C}e^{-M^2/2\chi} , \tag{B1}$$

where $P(\mathbf{M})$ is the probability for a system configuration to have magnetization $\mathbf{M}$, χ is the total uniform susceptibility, and $\mathcal{C}$ is the normalization constant determined from the condition that $\int P(\mathbf{M})d\mathbf{M}=1$.
Now

$$\langle C_{\mathbf{q}=0}\rangle=\frac{1}{N}\langle M^2\rangle . \tag{B2}$$

Let us denote $C_{\mathbf{q}=0}$ by C_0,

$$\langle(C_0-\langle C_0\rangle)^2\rangle=\frac{1}{N^2}(\langle M^4\rangle-\langle M^2\rangle^2) , \tag{B3}$$

$$\langle M^2\rangle=\frac{\int M^2P(\mathbf{M})d\mathbf{M}}{\int P(\mathbf{M})d\mathbf{M}} , \tag{B4}$$

$$\langle M^4\rangle=\frac{\int M^4P(\mathbf{M})d\mathbf{M}}{\int P(\mathbf{M})d\mathbf{M}} . \tag{B5}$$

The calculation is straightforward now. One gets,

$$\langle M^2\rangle=3\chi ,$$
$$\langle M^4\rangle=15\chi^2 .$$

Therefore

$$\frac{(C_0)_{rmsf}}{\langle C_0\rangle}=\frac{(\langle M^4\rangle-\langle M^2\rangle^2)^{1/2}}{\langle M^2\rangle}$$
$$=\frac{(6\chi^2)^{1/2}}{3\chi}=\sqrt{\tfrac{2}{3}}\simeq0.8165 .$$

This result was used to check the attainment of thermal equilibrium distribution for spin configurations in our MC calculation, as mentioned earlier.

APPENDIX C: DERIVATION OF THE PARAMETERS IN RITCHIE-FISHER FORM

We use a slightly nonstandard form of the Ritchie-Fisher formula which is elaborated here. This was used by Shastry in the iron problem. The function has too many unknown parameters and is inconvenient for use directly. Making use of a few simple relations, we reduce the number of unknown parameters occurring in the function.
The functional form, mentioned earlier, is

$$(C_q)_{av}=\frac{\alpha(\beta+\gamma\psi_q)^{\eta/2}}{\beta+\psi_q} , \tag{C1}$$

where ψ_q is the characteristic function which determines the spin-wave dispersion relation at very low temperature.

$$\psi_q\propto\mathcal{J}(0)-\mathcal{J}(\mathbf{q}) ,$$

where $\mathcal{J}(\mathbf{q})$ is the Fourier transform of $J_{ij}\equiv J(|\mathbf{r}_i-\mathbf{r}_j|)$ and $\mathcal{J}(0)\equiv\mathcal{J}(\mathbf{q}=0)$. Now

$$\psi_q=\psi_{1q}+\phi\cdot\psi_{2q} ,$$

where all the symbols have been explained earlier in the main text in Eqs. (3.15)-(3.17). For small q, we can expand ψ_{1q} and ψ_{2q} to get

$$\psi_q\simeq\frac{q^2a^2}{12}(1+2\phi) . \tag{C2}$$

Thus combining (C2) and (C1) we get for small q,

$$C_q\simeq C_0\left[1-p\left[1-\frac{\eta\gamma}{2}\right]\right] ,$$

where

$$C_0\equiv C_{\mathbf{q}=0}=\alpha\cdot\beta^{\eta/2-1}$$

and

$$p=\frac{q^2a^2}{12\beta}(1+2\phi) .$$

Thus

$$\frac{C_q}{C_0} = 1 - p\left[1 - \frac{\eta\gamma}{2}\right] . \tag{C3}$$

Again for a system with purely ferromagnetic interactions, C_q as a function of q shows a maximum at $q = 0$. Then for low q we can write (by Taylor's expansion about $q = 0$)

$$C_q \simeq C_0 - \delta q^2$$

$$= \int C(r)d\mathbf{r} - \frac{q^2}{6}\int r^2 C(r)d\mathbf{r} , \tag{C4}$$

where

$$\delta = \tfrac{1}{6}\int r^2 C(r)d\mathbf{r} ,$$

$$\therefore \frac{C_q}{C_0} = 1 - \frac{\delta q^2}{C_0} . \tag{C5}$$

Comparing (C3) and (C4) we get,

$$\frac{a^2}{12\beta}(1+2\phi)\left[1 - \frac{\eta\gamma}{2}\right] = \frac{\delta}{C_0} . \tag{C6}$$

The usual asymptotic form for $C(r)$, viz.

$$C(r) \sim \frac{e^{-r/\xi}}{r^{d-2+\eta}} ,$$

gives from (C4) , \hfill (C7)

$$\frac{\delta}{C_0} = \frac{\xi^2}{6}(6 - 5\eta + \eta^2) .$$

Now from (C6) and (C7) and neglecting η, we get

$$\xi^2 = \frac{a^2(1+2\phi)}{12\beta} .$$

Using this expression of ξ^2, from (C6) and (C7), we get

$$\gamma = \frac{5-\eta}{3} = 1.65 \quad (\text{since } \eta = \tfrac{2}{45} = 0.04) .$$

Also by the sum rule

$$\frac{1}{N}\sum_q C_q = S(S+1) ,$$

we get

$$\alpha = [NS(S+1)] \bigg/ \left[\sum_q (\beta + \gamma\psi_q)^{\eta/2}/(\beta + \psi_q)\right] .$$

Thus we have reduced the four-parameter $(\alpha,\beta,\gamma,\eta)$ system to simply one parameter, viz. β which remains as the fitting parameter in the parametrization process.

APPENDIX D: FWHM OF TUKEY WINDOW

As mentioned earlier in the text, the finite-time truncation in the time evolution in the MD leads to a spectral distortion, viz. the appearance of lots of ripples in the computed structure function $S(q,\omega)$. In order to reduce this spectral distortion, we will have to multiply $C_q(t)$ with a suitable spectral smoothing function which vanishes smoothly (with zero slope) at the two ends of the finite-time interval. We use the Tukey function which is quite popular in the field of spectral analysis. Its Fourier transform, known as the Tukey window, is very much like a Gaussian function. By the convolution theorem, the full width at half maximum of the Tukey window is a measure of the total amount of the spectral distortion produced and is quoted as a resolution width.

If the duration of the data recording (in our case the duration of the MD evolution) is from $-t_{max}/2$ to $+t_{max}/2$, then the corresponding Tukey function is defined as

$$R(t) = 0.5[1 + \cos(2\pi t/t_{max})] \quad \text{for} \quad |t| \leq t_{max}/2 ,$$

$$R(t) = 0 \quad \text{for} \quad |t| > t_{max}/2 .$$

The Fourier transform of $R(t)$ is the spectral window $W(\omega)$ which decides the distortion of the observed spectrum from the ideal one. The Fourier transformation of $R(t)$ gives,

$$W(\omega) = \frac{1}{2\pi}\int_{-t_{max}/2}^{+t_{max}/2} 0.5[1 + \cos(2\pi t/t_{max})]e^{i\omega t}dt$$

or

$$W(\omega) = \frac{1}{4\pi}\sin\left[\frac{\omega t_{max}}{2}\right]\left[\frac{2}{\omega} - \frac{1}{\omega + \frac{2\pi}{t_{max}}} - \frac{1}{\omega - \frac{2\pi}{t_{max}}}\right] .$$

This shows that

$$W(0) = \frac{t_{max}}{4\pi} ,$$

$$W\left[\pm\frac{2\pi}{t_{max}}\right] = \frac{t_{max}}{8\pi} .$$

Thus

$$\mathcal{W}_{FWHM} = \frac{4\pi}{t_{max}}$$

in units of ω. So in energy units,

$$\mathcal{W}_{FWHM} = \frac{4\pi\hbar}{t_{max}}$$

$$= \frac{2h}{t_{max}} .$$

[1] P. Böni and G. Shirane, Phys. Rev. B **33**, 3012 (1986).

[2] R. A. Tahir-Kheli, in *Phase Transitions and Critical Phenomena*, edited by C. Domb and M. S. Green (Academic, New York, 1976), Vol. 5b, Chap. 4.

[3] S. W. Lovesey, *Theory of Neutron Scattering From Condensed Matter* (Clarendon, Oxford, 1984), Vol. 2, Chap. 9.

[4] A. P. Young and B. S. Shastry, J. Phys. C **15**, 4547 (1982).

[5] Per-Anker Lindgard, J. Appl. Phys. **53**, 1861 (1982); Phys. Rev.

B 27, 2980 (1983).

[6]B. Sriram Shastry, D. M. Edwards, and A. P. Young, J. Phys. C 14, L665 (1981).

[7]H. A. Mook, Phys. Rev. Lett. 46, 508 (1981).

[8]Ranjan Chaudhury and B. S. Shastry (unpublished).

[9]B. Sriram Shastry, Phys. Rev. Lett. 53, 1104 (1984).

[10]P. Resibois and M. De Leener, Phys. Rev. 178, 806 (1969).

[11]R. Folk and H. Iro, Phys. Rev. B 32, 1880 (1985).

[12]P. C. Hohenberg and B. I. Halperin, Rev. Mod. Phys. 49, No. 3 (1977).

[13]K. Kawasaki, in Phase Transitions and Critical Phenomena, edited by C. Domb and M. S. Green (Academic, New York, 1976), Vol. 5a, Chap. 4.

[14]M. Blume and J. Hubbard, Phys. Rev. 81, 3815 (1970).

[15]G. F. Reiter, Phys. Rev. B 7, 3325 (1973).

[16]S. W. Lovesey and R. A. Meserve, J. Phys. C 6, 79 (1973).

[17]H. Mori, Prog. Theor. Phys. 33, 423 (1965); 34, 399 (1965).

[18]G. S. Joyce, in Phase Transitions and Critical Phenomena, edited by C. Domb and M. S. Green (Academic, New York, 1972), Vol. 2, Chap. 10.

[19]M. T. Evans and C. G. Windsor, J. Phys. C 6, 495 (1973).

[20]N. Metropolis, A. W. Rosenbluth, M. N. Rosenbluth, A. H. Zeller, and E. Zeller, J. Chem. Phys. 21, 1089 (1953).

[21]R. E. Watson, M. Blume, and G. Vineyard, Phys. Rev. 181, 811 (1969).

[22]R. D. Ritchie and M. E. Fisher, Phys. Rev. B 5, 2668 (1972).

[23]M. Takahashi, J. Phys. Soc. Jpn. 52, 3592 (1983).

[24]S. Gill, Proc. Cambridge Philos. Soc. 47, 96 (1951).

[25]G. Jenkins and D. Watts, Spectral Analysis and its Applications (Holden-Day, San Francisco, 1968).

[26]J. Als Nielsen, in Phase Transitions and Critical Phenomena, edited by C. Domb and M. S. Green (Academic, New York, 1976), Vol. 5A, Chap. 3.

[27]D. W. Wood and N. W. Dalton, Phys. Rev. 159, 384 (1967).